Cross sections of the ^{91}Zr$(n, \alpha)^{88}$Sr reaction in the 3.9–5.3 MeV neutron energy region

Guohui Zhang,[1] E. Sansarbayar,[2,3,*] Yu. M. Gledenov,[2] G. Khuukhenkhuu,[3] L. Krupa,[4,5] N. S. Gustova,[4] M. G. Voronyuk,[4] I. Chuprakov,[2,6,7] N. Battsooj,[3] I. Wilhelm,[5] M. Solar,[5] R. Sykora,[5] Z. Kohout,[5] Jie Liu,[1] Yiwei Hu,[1] and Zengqi Cui[1]

[1]*State Key Laboratory of Nuclear Physics and Technology, Institute of Heavy Ion Physics, School of Physics, Peking University, Beijing 100871, China*

[2]*Frank Laboratory of Neutron Physics, Joint Institute for Nuclear Research, Dubna 141980, Russia*

[3]*Nuclear Research Center, National University of Mongolia, Ulaanbaatar 210646, Mongolia*

[4]*Flerov Laboratory of Nuclear Reactions, Joint Institute for Nuclear Research, Dubna 141980, Russia*

[5]*Institute of Experimental and Applied Physics, Czech Technical University in Prague, Husova 240/5, Prague 1, 110 00, Czech Republic*

[6]*Faculty of Physics and Technology, L.N. Gumilyov Eurasian National University, Nur-sultan 010000, Kazakhstan*

[7]*The Institute of Nuclear Physics, Ministry of Energy of the Republic of Kazakhstan, Almaty 050032, Kazakhstan*

(Received 20 July 2022; accepted 17 November 2022; published 8 December 2022)

Cross sections of the ^{91}Zr$(n, \alpha)^{88}$Sr reaction were measured at four incident neutron energies in the range of 3.9 to 5.3 MeV. The experiment was carried out on the Van de Graaff accelerator EG-5 at the Frank Laboratory of Neutron Physics, Joint Institute for Nuclear Research, Russia. Fast neutrons were produced via the ^{2}H$(d, n)^{3}$He reaction with a deuterium gas target. A twin gridded ionization chamber (GIC) was used as the charged particle detector, in which ^{91}Zr back-to-back samples on a tantalum backing were placed at the common cathode. The relative and absolute neutron fluxes were measured using two $^{238}U_3O_8$ samples inside the GIC. Cross-section data obtained in this measurement were compared with those in existing data library and from theoretical calculations using TALYS code. The present data for the ^{91}Zr$(n, \alpha)^{88}$Sr reaction should be helpful in clarifying the discrepancies in various published nuclear evaluation data. An alpha clustering factor is calculated using the statistical model and knock-on mechanism.

DOI: 10.1103/PhysRevC.106.064602

I. INTRODUCTION

Studies of neutron-induced reactions with the emission of charged particles are important for nuclear physics and technology. Zirconium isotopes can be produced by neutron-induced fission and are close to the peak yield of light-mass fragments.

Zirconium is a structural element in reactor systems. Zirconium alloys are used in fuel rods of fission reactors for their low neutron absorption cross section. In addition, zirconium is used in the blanket and first wall of fusion reactors because of its resistance to high temperatures. Therefore, reliable nuclear data for Zr isotopes are needed. Natural zirconium contains five stable isotopes, which are ^{90}Zr (51.45%), ^{91}Zr (11.22%), ^{92}Zr (17.15%), ^{94}Zr (17.38%), and ^{96}Zr (2.80%). For ^{92,94,96}Zr(n, α) reactions, it is possible to carry out measurements with the activation method, since the daughter nuclei are radioactive [1–4]. In the case of ^{91}Zr, the measurement of the (n, α) reaction cross section is possible only by direct detection of α particles because the ^{88}Sr daughter nucleus is stable. The same situation holds for ^{90}Zr. Currently, there are no cross section data for the ^{91}Zr$(n, \alpha)^{88}$Sr reaction in the MeV neutron energy region. For this reaction only one measurement exist at two neutron energy points around 14 MeV [5]. Moreover, in the 3.9 MeV $\leqslant$ En $\leqslant$ 5.3 MeV energy region, the evaluated cross section in the ENDF/B-VIII.0 [6], JENDL-5.0 [7], CENDL-3.2 [8], ENDF/B-VII.0 [9], JEFF-3.3 [10], BROND-3.1 [11], and TENDL-2019 [12] libraries differ by up to 6.4 times. In this work we carried out cross-section measurements for the ^{91}Zr$(n, \alpha)^{88}$Sr reaction in the energy range of 3.9 to 5.3 MeV utilizing direct detection method with the help of a twin gridded ionization chamber (GIC).

II. DETAILS OF EXPERIMENTS

The measurements were carried out on the EG-5 Van de Graaff accelerator at the Frank Laboratory of Neutron Physics, Joint Institute for Nuclear Research, Russia (FLNP JINR). The setup of the experiment is shown in Fig. 1 which includes three parts: The neutron source, the twin gridded ionization chamber (GIC), and the ^{3}He counter.

A. Neutron source

Fast neutrons were produced via the ^{2}H$(d, n)^{3}$He reaction using a deuterium gas target. The gas cylinder vessel 2.0 cm in length and 0.9 cm in diameter separated from the vacuum tube of the accelerator by molybdenum foil 6.0 μm in

*sansar@nf.jinr.ru

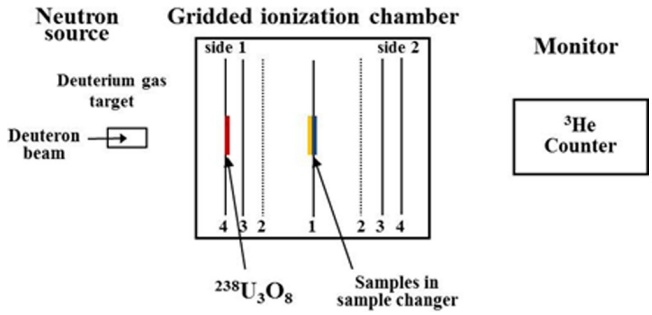

FIG. 1. Scheme of the experimental setup. 1, 2, 3-common cathode with samples, grids, and anodes of the gridded twin ionization chamber (GIC), respectively; 4-fission chamber (FC) cathode.

thickness. The pressure of the deuterium gas was 2.5 atm, and the incident deuterium beam current was approximately 2.5 μA. The energy range of the incident deuterons was 1.6–2.8 MeV to generate neutrons with energy 3.9–5.3 MeV.

B. Charged particle detector, data-acquisition system, and samples

The twin gridded ionization chamber (GIC) with a common cathode, supplemented by a fission chamber, is used as a charged particle detector. The structure of the GIC and its characteristics were presented in Ref. [13]. The distances between the GIC electrodes were as follows: Cathode-grid 6.1 cm; grid-anode 1.8 cm; FC anode-cathode 1.0 cm. The distance from the edge of the deuterium target to the cathode of the GIC was 15.4 cm. Kr + 4% CH_4 and Kr + 3% CO_2 were used as the working gas at a pressure of 1.3 atm, so the alpha particles can be stopped before reaching the grids. The grid electrodes were grounded, the high voltage applied to the anodes was +1000 V, and to the cathode −1500 V. The cathode and anodes were covered with tantalum foil to reduce the background. The detector signals were recorded using a 14-bit Pixie-16 module with a sampling frequency of 250 MHz. The Pixie system consists of a chassis (PXI-6023 XIA 14, Wiener), an embedded controller (NI PXI-8820), and a high-speed digitizer (Pixie-16).

A sample changer with five sample positions was set at the common cathode of the GIC. The device of the sample changer allows us to change the samples without opening the GIC. The samples used in the present measurements were as follows: (1) natural uranium α sources (E_α = 4.197 and 4.775 MeV) for energy calibration and verification of the functioning of the GIC; (2) a pair of ^{91}Zr samples; (3) ^{238}U sample for measurement of the neutron flux; and (4) pure Ta foils to measure the background events. All the samples were deposited on Ta substrates 48 mm in diameter and 0.10 mm in thickness. Characteristics of the ^{91}Zr and ^{238}U samples are given in Table I. The content of Zr isotopes in the samples are ^{90}Zr (2.19%), ^{91}Zr (95.50%), ^{92}Zr (1.74%), ^{94}Zr (0.51%), and ^{96}Zr (0.06%).

Samples with supposed chemical composition ZrO_2 were prepared in three layers by modified molecular plating method followed by calcination at 450 °C. Electrodeposition took place in isopropanol with addition of aliquot zirconium solution at oxalic acid at tantalum anode under 0.26–1.25 mA/cm^2 current density and 990 V voltage for 75 minutes at room temperature. The XRF method was used to determine the target thickness.

TABLE I. Characteristics of samples.

Sample	Abundance (%)	Thickness(μg/cm^2)	Diameter (mm)
$^{91}ZrO_2$ 01	95.50	370 ± 20[a]	44.0
$^{91}ZrO_2$ 02	95.50	390 ± 20[a]	44.0
$^{238}U_3O_8$ 01[b]	99.999	411.0	44.0
$^{238}U_3O_8$ 02[c]	99.999	475.0	44.0

[a]Thickness of zirconium only.
[b]Sample on the FC cathode.
[c]Sample on the GIC cathode.

C. Neutron flux measurement and monitor

The absolute neutron flux was determined from the registration of fission fragments of ^{238}U, installed in one of the five sample positions at the GIC common cathode. A fission chamber ("4" in Fig. 1) and a ^{3}He long counter were used as neutron flux monitors.

D. Simulation of measurements of the ^{91}Zr(bn, α)^{88}Sr reaction

Before measurements, we performed calculations to predict the experimental spectra of the ^{91}Zr$(n,\alpha)^{88}$Sr reaction and possible interference reactions, including (n, p), (n,α) reactions of Kr, O, N (from the air), ^{1}H(n, p). Calculations were carried out using the MATLAB computer code, using cross sections, angular and energy distributions from TALYS-1.9 [14] and the geometry according to Fig. 1. Simulations were carried out for solid sample of zirconium with a thickness of 390 μg/cm^2 and working gas Kr + 4% CH_4 at a pressure of 1.3 atm. The calculations were made for the neutron energy range 3.9–5.3 MeV. The calculations determined the expected positions of events for the studied reaction, as well as background reactions that can mask the effect. Figures 2 and 3 show the calculated two-dimensional cathode-anode spectrum of α particles from the ^{91}Zr$(n,\alpha)^{88}$Sr reaction at E_n = 5.3 MeV, emitted from a zirconium sample in the "forward" and "backward" direction along the neutron beam, respectively, and the influence of background reactions is also indicated. The contribution from the reaction of nitrogen was estimated, the presence of a small amount of which is possible in the GIC from the air. It is shown that this is an interfering factor and measures were taken to clean the GIC before filling it with working gas, and gases of special purity were also used.

III. MEASUREMENTS of THE ^{91}Zr(n, α)^{88}Sr REACTION WITH FAST NEUTRONS

A. Experimental procedure

Two series of measurements were carried out: (1) with a working gas of Kr + 4% CH_4 at the neutron energies of 4.3;

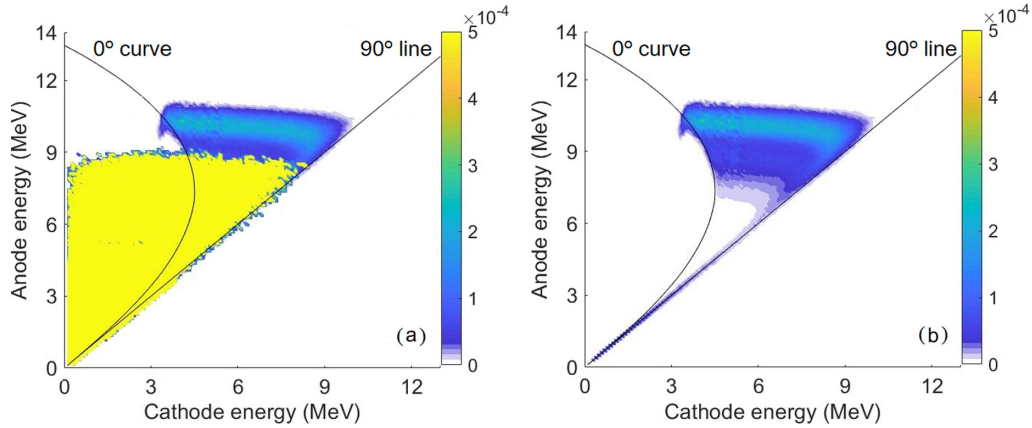

FIG. 2. Calculated two-dimensional cathode-anode two-dimensional spectra of α particles from the ^{91}Zr$(n,\alpha)^{88}$Sr reaction at $E_n = 5.3$ MeV in the "forward" direction: (a) taking into account all possible background reactions; (b) taking into account only "pure" events.

5.0 and 5.3 MeV and (2) with a working gas of Kr + 3% CO_2 at neutron energies of 3.9 and 4.3 MeV. At each neutron energy point, the following measurement runs were performed: Calibration using the alpha source; measurement with back-to-back ^{91}Zr samples; measurement of the neutron flux using ^{238}U(n,f); background measurement with pure Ta backings; recalibration from alpha source. The signals from the fission fragments of the FC were fed into the data-acquisition system when measuring the foreground, background, and ^{238}U(n,f) reaction. ^{91}Zr samples were irradiated for 12 to 24 h, depending on the neutron flux density at different neutron energies. The absolute neutron flux was measured for each neutron energy in a separate measurement using the ^{238}U(n,f) reaction by placing a uranium sample ("$^{238}U_3O_8$02" in Table I) of exactly the same dimensions and in the same position in which the investigated samples are placed. In this case, the FC and the long ^{3}He counter, which serve to monitor the neutron flux, were calibrated. All of these monitoring methods gave very close values, so in what follows we use the data obtained using the FC.

The total fission counts from the "$^{238}U_3O_8$02" sample were used to determine the absolute neutron flux. A typical anode spectrum of the fission fragments is shown in Fig. 4 as an example.

The cathode-anode two-dimensional spectra have been analyzed. Figures 5 and 6 show the two-dimensional spectra for foreground and background measurements of the ^{91}Zr$(n,\alpha)^{88}$Sr reaction in the forward and backward direction at $E_n = 5.3$ MeV, respectively. Figure 7 shows the anode projection spectra of the foreground, background, and net events together with the simulation spectra for the measurement of the ^{91}Zr$(n,\alpha)^{88}$Sr reaction in the forward [Fig. 7(a)] and backward [Fig. 7(b)] directions at $E_n = 5.3$ MeV, respectively.

The cross section of the ^{91}Zr$(n,\alpha)^{88}$Sr reaction $\sigma_{n,\alpha}$ was obtained using the following formula:

$$\sigma_{n,\alpha} = K\sigma_{n,f}\frac{N_\alpha}{N_f}\frac{\epsilon_f}{\epsilon_\alpha}\frac{N_{^{238}\mathrm{U}}}{N_{^{91}\mathrm{Zr}}}, \tag{1}$$

where $K = \frac{\mathrm{Fis}_f}{\mathrm{Fis}_\alpha}$; Fis_α and Fis_f are fission-fragment counts of the fission chamber while the ^{91}Zr$(n,\alpha)^{88}$Sr and ^{238}U(n,f) reactions were measured, respectively. $\sigma_{n,f}$ is the ^{238}U(n,f) reactions cross section taken from ENDF/B-VIII.0 [6]. N_α

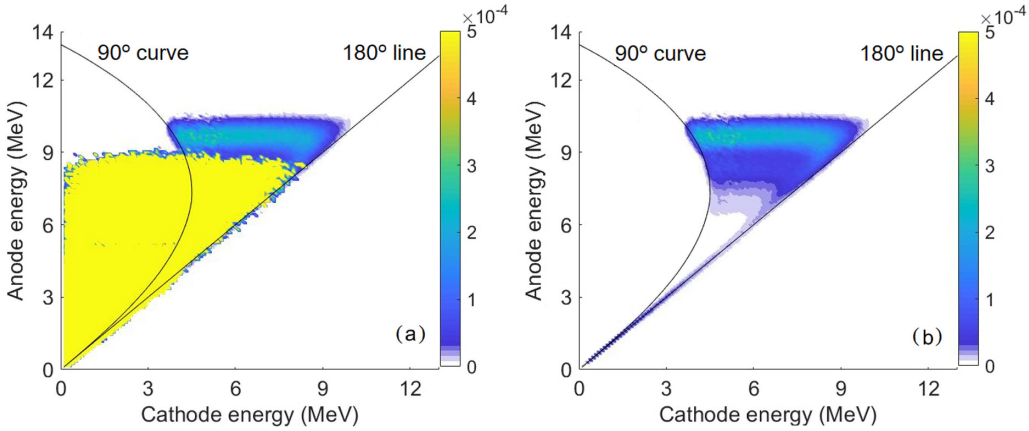

FIG. 3. The same as Fig. 2 but for the "backward" direction.

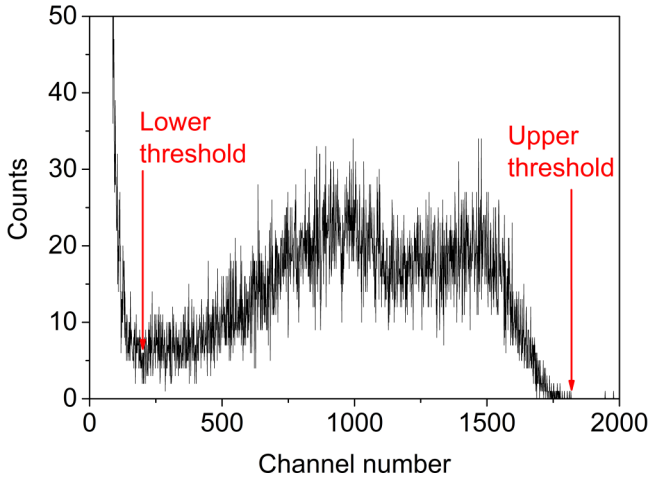

FIG. 4. The anode spectrum of fission fragments for measuring the absolute neutron flux of the ^{238}U(n, f) reaction at $E_n = 5.3$ MeV.

and N_f are the numbers of pure alpha and fission events within the lower and higher thresholds in the ^{91}Zr$(n, \alpha)^{88}$Sr and ^{238}U(n, f) reactions. Influences of the alpha particles from minor isotopes in the samples are ignored because the energy of the influenced alpha particles are all different from the ^{91}Zr$(n, \alpha)^{88}$Sr reaction. ϵ_f and ϵ_α are detection efficiencies of the fission and alpha events. $N_{^{238}\mathrm{U}}$ and $N_{^{91}\mathrm{Zr}}$ are the atom numbers of the ^{238}U and ^{91}Zr samples, respectively. The detection efficiencies of the fission events (ϵ_f) and alpha events (ϵ_α) are calculated using Monte Carlo simulation. Details of which are described in Ref. [15]. The values of (ϵ_f) and (ϵ_α) are 90% and 94%, respectively.

B. Results and discussions

Experimental cross sections of the ^{91}Zr$(n, \alpha)^{88}$Sr reaction were obtained from formula (1). The cross-section uncertainties at four energies were calculated by adding uncertainties listed in Table II. Uncertainty of the total ^{91}Zr$(n, \alpha_0)^{88}$Sr cross section was in the range of 9% to 16%.

The measured (n, α_0) cross section can be obtained by summing up the forward and the backward cross sections. In our experiment, only α_0 particles were measured, which leaves the residual nucleus in the ground state. The cross section of the (n, α_1) reaction in the first-excited state is calculated using the ratio of the cross sections of the ground state and the first-excited state of the residual nucleus calculated with TALYS-1.9 [14] adjusted parameters. ^{91}Zr$(n, \alpha)^{88}$Sr reaction cross sections corresponding to the second-excited states of ^{88}Sr are small and their contribution to the total cross section is insignificant. The results are shown in Table III. Total (n, α) cross sections are shown in Fig. 8 from our measurement and TALYS-1.9 calculations with adjusted parameters (listed in Table IV). Present cross sections of the ^{91}Zr$(n, \alpha)^{88}$Sr reaction were compared with nuclear data from different evaluation libraries [6–12] and calculation results using TALYS-1.9. The present cross sections are 1.2–3.2 times lower than the evaluations of the ENDF/B-VIII.0 [6], JENDL-5.0 [7], and JEFF-3.3 [10]. The difference between our results and CENDL-3.2 [8] and TENDL-2019 [12] evaluations is 14%–33%. The ENDF/B-VII.0 [9] evaluation satisfactorily describes our results excepting at neutron energy of 4.3 MeV. The present results are in agreement with BROND-3.1 [11] evaluation in the neutron energy range of 5.0 and 5.3 MeV. In addition, our experimental cross sections of the (n, α) reaction are in good agreement with TALYS-1.9 calculations with adjusted parameters excepting at 3.9 MeV where our datum is less than 20%.

IV. ALPHA-CLUSTERIZATION EFFECT IN THE ^{91}Zr$(n, \alpha)^{88}$Sr REACTION

An important issue related to the α decay and (n, α) reaction is how to estimate the α-cluster preformation (or α clustering) factor Φ_α that is defined as the probability of finding an alpha particle inside the parent nucleus. In the case of the (n, α) reaction an additional painful situation arises when an α particle is formed before or after interaction of neutrons with target nuclei. In this section we try to estimate the

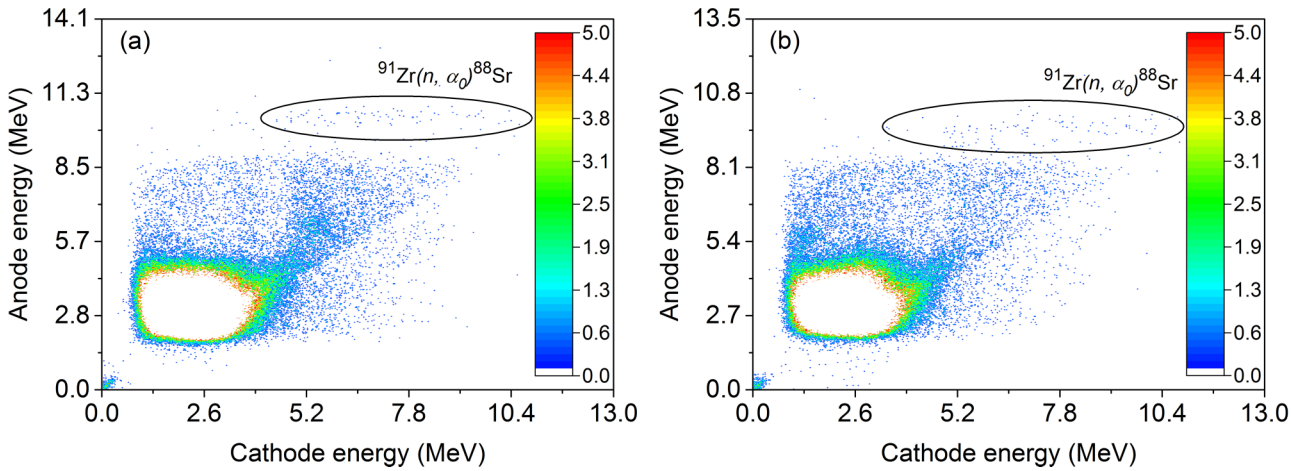

FIG. 5. Two-dimensional foreground spectra of the ^{91}Zr$(n, \alpha)^{88}$Sr reaction in the (a) forward and (b) backward directions for $E_n = 5.3$ MeV.

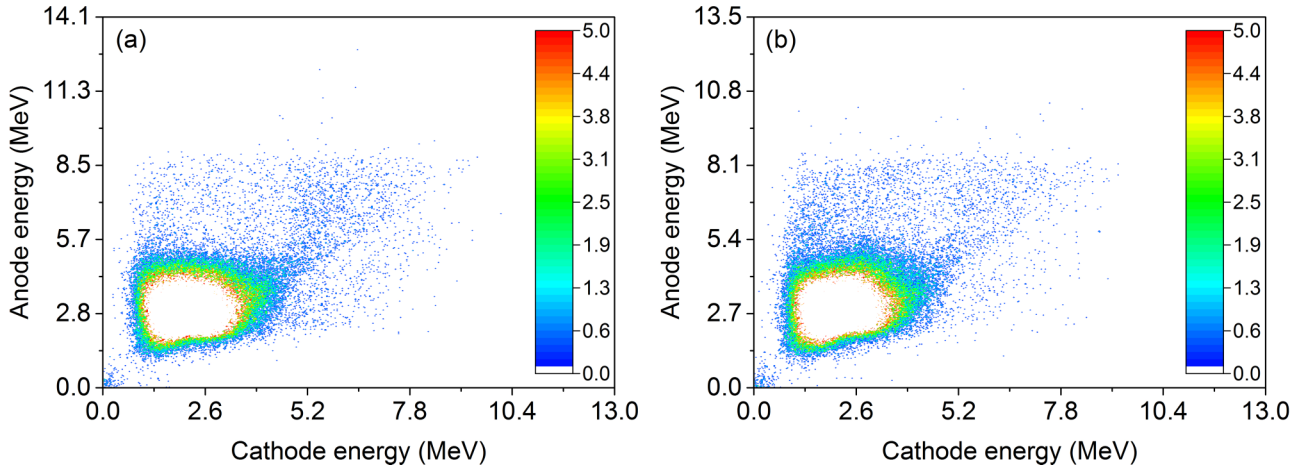

FIG. 6. Two-dimensional background spectra of the $^{91}\mathrm{Zr}(n,\alpha)^{88}\mathrm{Sr}$ reaction in the (a) forward and (b) backward directions at $E_n = 5.3$ MeV.

α-clustering factor in the $^{91}\mathrm{Zr}(n,\alpha)^{88}\mathrm{Sr}$ reaction to elucidate the above-mentioned problems using the compound mechanism and knock-on model.

A. The statistical model approach

According to the statistical model based on Bohr's conception of a compound mechanism and taking into account the α-clusterization effect, the (n,α) reaction cross section can be written as a three stages process:

$$\sigma_{n\alpha}^{\mathrm{stat}} = \sigma_c(n)\Phi_\alpha G(\alpha), \tag{2}$$

where $\sigma_c(n) = \pi(R+\lambda\!\!\!^{-})^2$ is the compound nucleus formation cross section, R is the radius of the target nucleus, $\lambda\!\!\!^{-}$ is the wavelength of the incident neutrons divided by 2π; Φ_α is the α-cluster formation factor and $G(\alpha)$ is the α-particle emission probability from the compound nucleus. In this case it is assumed that the α cluster is formed after interaction of neutrons with target nuclei and before emission of the α particle from the compound nucleus. The α-particle emission probability is given by [16]

$$G(\alpha) = \frac{\Gamma_\alpha}{\Gamma}, \tag{3}$$

where Γ is the total level width for the compound nucleus and Γ_α is the decay width for the α emission. For fast neutrons the total level width can be approximately taken as $\Gamma \approx \Gamma_n$, where Γ_n is the neutron decay width. The alpha particle and neutron decay widths can be determined [17] using the evaporation model and constant-temperature approximation [16]. Then, using Weizsäcker's formula for binding energy, the (n,α) cross section can be obtained [17]:

$$\sigma_{n\alpha}^{\mathrm{stat}} = C\pi(R+\lambda\!\!\!^{-})^2\Phi_\alpha \exp\left(-K\frac{N-Z+0.5}{A}\right), \tag{4}$$

where $A = N+Z$, N, and Z are the neutron and proton numbers of the target nuclei, respectively; C and K are fitting

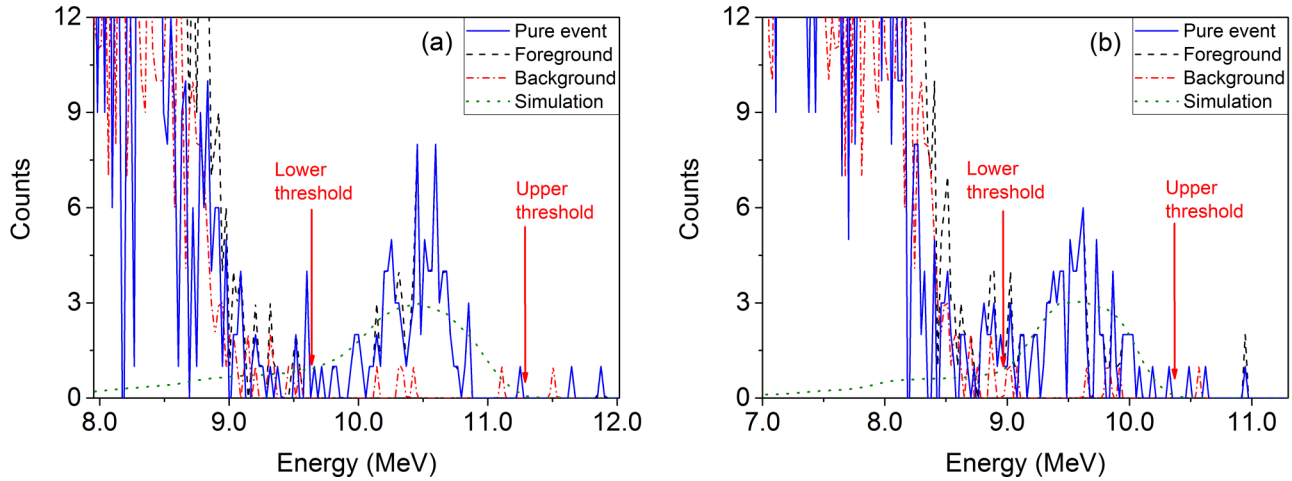

FIG. 7. The anode projection spectra of the $^{91}\mathrm{Zr}(n,\alpha)^{88}\mathrm{Sr}$ reaction in the (a) forward and (b) backward directions at $E_n = 5.3$ MeV, respectively.

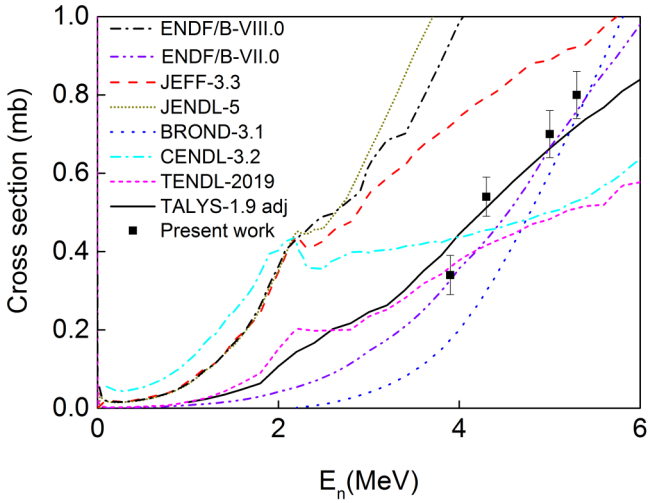

FIG. 8. Present experimental cross sections of the ^{91}Zr$(n,\alpha)^{88}$Sr reaction compared with the results from evaluations and using TALYS-1.9.

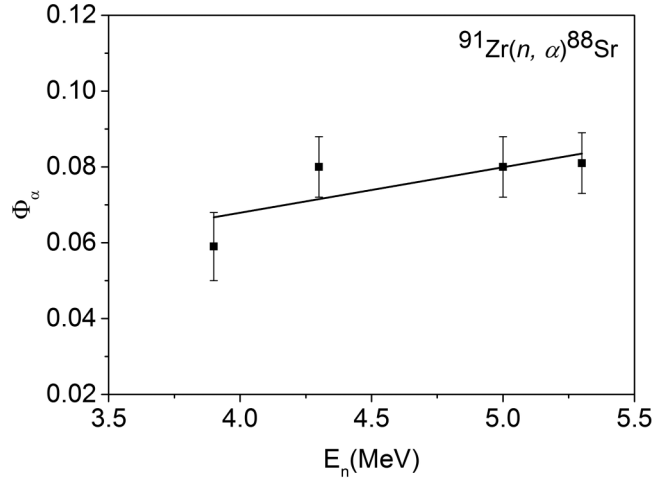

FIG. 9. Alpha-clustering factor calculated with the statistical model as a function of the neutron energy for the ^{91}Zr$(n,\alpha)^{88}$Sr reaction.

parameters, which can be determined as follows:

$$C = 2\exp\frac{1}{\Theta}\left\{-3\alpha+\beta[A^{2/3}-(A-3)^{2/3}] + \gamma\left[\frac{Z^2}{A^{1/3}}-\frac{(Z-2)^2}{(A-3)^{1/3}}\right] \pm\left[\frac{\delta_f}{(A-3)^{3/4}}-\frac{\delta_i}{A^{3/4}}\right]+\epsilon_\alpha - V_\alpha\right\}, \quad (5)$$

and

$$K = \frac{2\xi}{\theta}, \quad (6)$$

where α, β, γ, ξ, and $\delta_{i,f}$ are Weizsäcker's constants; $\epsilon_\alpha = 28.3$ MeV is the internal binding energy of the α particle; $\theta = kT$ is the thermodynamical temperature; k is the Boltzmann constant; T is the absolute temperature. The nuclear thermodynamical temperature can be determined via the level-density parameter [16,17]. V_α is the Coulomb potential energy of α particles [17,18]. In the one-body approximation [19,20] it can be assumed that the α-clustering factor $\Phi_\alpha = 1$. Then, in the framework of the statistical model the α-clustering factor can be determined from Eq. (4) via experimental (n,α) cross section, $\sigma_{n\alpha}^{\rm expt}$, by analogy with the spectroscopic factor [20] as follows:

$$\Phi_\alpha = \frac{\sigma_{n\alpha}^{\rm expt}}{\sigma_{n\alpha}^{\rm stat}(\Phi_\alpha=1)} = \frac{\sigma_{n\alpha}^{\rm expt}}{C\pi(R+\lambda\!\!\!^{-})^2\exp\left(-K\frac{N-Z+0.5}{A}\right)}. \quad (7)$$

Results of the α-clustering factor calculated using Eqs. (5)–(7) for the ^{91}Zr$(n,\alpha)^{88}$Sr reaction in the range of 3.9 to 5.3 MeV are shown in Fig. 9. The experimental (n,α) cross sections were taken from Table III. It can be seen that the α-clustering factor is slightly increased from 0.059 to 0.081 as the incident neutron energy increase from 3.9 to 5.3 MeV.

TABLE II. Sources of the uncertainty.

Source	Magnitude (%)
$N_{^{238}\rm U}$	2.0[a]
$N_{^{91}\rm Zr}$	3.0[b]
$\sigma_{n,f}$	0.7[b]
Fis$_f$	3.0[b]
Fis$_\alpha$	3.0[b]
N_α	10.0–15.0[b]
N_f	3.0[b]
σ_α	9.0–16.0[b]
ϵ_α	2.0[b]
ϵ_f	2.0[b]

[a]For the forward or backward cross sections.
[b]For the total cross section (forward cross section + backward cross section).

B. The knock-on model

In the framework of the direct reaction mechanism using the knock-on model the (n,α) cross section can be expressed as a two-stage process:

$$\sigma_{n\alpha} = \Phi_\alpha\sigma_n^{\rm tot}(^4{\rm He}), \quad (8)$$

where Φ_α is the α-cluster preformation factor and $\sigma_n^{\rm tot}(^4{\rm He})$ is the total neutron cross section for the ^{4}He (or α particle). In this case it is assumed that the α cluster is preformed on the surface of the target nucleus before the interaction of the incident neutron with the target nucleus. From Eq. (8) the α-cluster preformation factor can be obtained as

$$\Phi_\alpha = \frac{\sigma_{n\alpha}}{\sigma_n^{\rm tot}(^4{\rm He})}, \quad (9)$$

TABLE III. Measured (n, α) cross sections for $^{91}Zr(n, \alpha)^{88}Sr$ reaction and results from TALYS-1.9.

	Cross sections (mb)				
Energy (MeV)	Forward (n, α_0)	Backward (n, α_0)	Measured (n, α_0)	Measured (n, α_0) + TALYS-1.9 (n, α_1)	TALYS-1.9 $(n, \alpha_{0,1})$
3.9	0.17 ± 0.03	0.15 ± 0.03	0.32 ± 0.05	0.34 ± 0.05	0.41
4.3	0.25 ± 0.03	0.24 ± 0.03	0.49 ± 0.05	0.54 ± 0.05	0.50
5.0	0.31 ± 0.04	0.28 ± 0.04	0.59 ± 0.06	0.7 ± 0.05	0.64
5.3	0.34 ± 0.04	0.31 ± 0.04	0.65 ± 0.06	0.8 ± 0.06	0.68

Results of the α-cluster preformation factor for the $^{91}Zr(n, \alpha)^{88}Sr$ reaction calculated using Eq. (9) are shown in Fig. 10.

In the calculations our experimental (n, α_0) cross sections for ^{91}Zr (see Table III) and total neutron cross sections for ^{4}He taken from EXFOR library [21] were utilized. It should be noted that in the calculations the total (n, α) cross section was assumed as $\sigma_{n\alpha} \approx \sigma(n, \alpha_0)$ for ^{91}Zr and $\sigma(n, \alpha_1) + \sigma(n, \alpha_2) + \cdots$ were neglected because the energy of the first-excited state of the daughter nucleus ^{88}Sr is 1.836 MeV and their contribution to the total $\sigma_{n\alpha}$ is insignificant. One can see from Fig. 10 that the α-cluster preformation factor calculated with the knock-on model for the $^{91}Zr(n, \alpha)^{88}Sr$ reaction is linearly increased from 1.28×10^{-4} to 2.98×10^{-4} as the incident neutron energy increase from 3.9 to 5.3 MeV. Furthermore, the α-cluster preformation factor obtained from the knock-on model is smaller than the α-clustering one from the compound mechanism by two orders of magnitudes. This shows that in the case of the $^{91}Zr(n, \alpha)^{88}Sr$ reaction for 3.9–5.3 MeV neutrons the α cluster is perhaps mostly formed after the interaction of incident neutrons with the target nucleus ^{91}Zr.

V. CONCLUSIONS

Cross sections of the $^{91}Zr(n, \alpha)^{88}Sr$ section were systematically measured with high accuracy at incident neutron energies of 3.9, 4.3, 5.0, and 5.3 MeV. The present data are the first experimental result in the MeV region. Measurements were performed using the EG-5 Van de Graaff accelerator, a GIC charged particle detector, enriched $^{91}ZrO_2$ samples and $^{238}U_3O_8$ samples. The total cross sections are obtained by adding the measured $^{91}Zr(n, \alpha_0)^{88}Sr$ cross sections and the partial (n, α_1) cross sections are calculated with the TALYS-1.9. Present cross sections of the $^{91}Zr(n, \alpha)^{88}Sr$ reaction were compared with the data from different evaluation libraries [6–12]. Our results are different from 14% to 3.2 times in comparison with the evaluations of the ENDF/B-VIII.0 [6], JENDL-5.0 [7], JEFF-3.3 [10], CENDL-3.2 [8], BROND [11], and TENDL-2019 [12]. The ENDF/B-VII.0 [9] evaluation and TALYS-1.9 calculations with adjusted parameters satisfactorily describe our results. In addition, the alpha clustering factor was calculated for the $^{91}Zr(n, \alpha)^{88}Sr$ reaction using two different methods. The obtained alpha clustering factors from compound mechanism are in average two orders of magnitudes higher than from knock-on mechanism. It means that the alpha cluster is formed after interaction of neutrons with target nucleus.

TABLE IV. Adjusted input parameters of the TALYS-1.9.

Keyword	Parameter
maxlevelsbin	a 30
ldmodel	2
alphaomp	3
Tljadjust	a 2.000 0
Tljadjust	a 2.00 1
Tljadjust	2.00 2
rvadjust	a 1.05
avadjust	a 0.2
aadjust	40 91 0.9
cstrip	a 0.3

ACKNOWLEDGMENTS

The authors are grateful to the operational team of the Van de Graaff accelerator EG-5 of the Frank Laboratory of Neutron Physics, JINR for kind cooperation. This work was supported by the LM2018108 project "Van de Graaff Accelerator - a Tunable Source of Monoenergetic Neutrons and Light Ions" of MEYS of the Czech Republic.

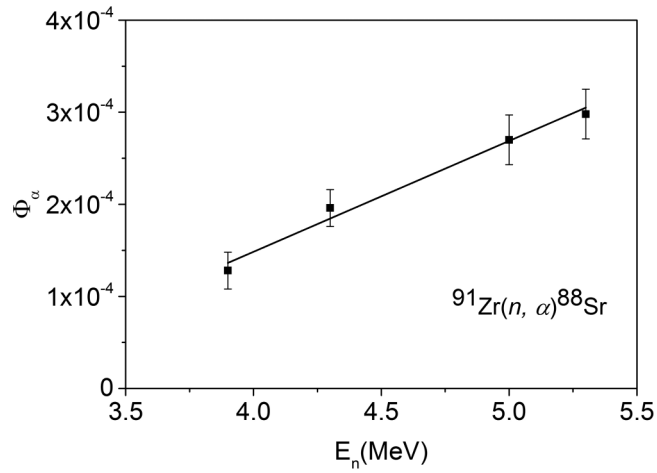

FIG. 10. Alpha-cluster preformation factor calculated with knock-on model as a function of the neutron energy for the $^{91}Zr(n, \alpha)^{88}Sr$ reaction.

[1] V. Semkova, E. Bauge, A. J. M. Plompen, and D. L. Smith, Nucl. Phys. A **832**, 149 (2010).
[2] M. I. Majah, A. Chiadli, S. Sudár, and S. M. Qaim, Appl. Radiat. Isot. **54**, 655 (2001).
[3] A. A. Filatenkov, S. V. Chuvaev, V. N. Aksenov and V. A. Jakovlev, Report No. INDC(CCP)-402, Vienna, 1997, https://www-nds.iaea.org/exfor/servlet/X4sShowPubl?File=R,INDC(CCP)-402,1997.
[4] V. N. Levkovskii, G. P. Vinitskaya, G. E. Kovelskaya, and V. M. Stepanov, Yadern. Fiz. **10**, 44 (1969) [Soviet J. Nucl. Phys. **10**, 25 (1970)].
[5] E. Gadioli, E. Gadioli Erba, L. Głowacka, M. Jaskoła, J. Turkiewicz, L. Zemło, J. Dalmas, and A. Chiadli, Phys. Rev. C **34**, 2065 (1986).
[6] Evaluated Nuclear Data File ENDF/B-VIII.0, http://www-nds.iaea.org/exfor/endf.html.
[7] Japanese Evaluated Nuclear Data Library JENDL-5.0, https://wwwndc.jaea.go.jp/jendl/j40/j40.html.
[8] Chinese Evaluated Nuclear Data Library CENDL-3.2, https://en.cnnc.com.cn/2020-06/17/c_501119.html.
[9] Evaluated Nuclear Data File ENDF/B-VII.0, https://www.nndc.bnl.gov/endf-b7.0.
[10] The Joint Evaluated Fission and Fusion File JEFF-3.3, https://www.oecd-nea.org/dbdata/jeff/jeff33/index.html.
[11] Neutron Evaluated Data Library BROND-3.1, https://vant.ippe.ru/en/brond-3-1.
[12] TALYS-based evaluated nuclear data library TENDL-2019, https://tendl.web.psi.ch/tendl_2019/tendl2019.html.
[13] G. Zhang, Yu. M. Gledenov, G. Khuukhenkhuu, M. V. Sedysheva, P. J. Szalanski, J. Liu, H. Wu, X. Liu, J. Chen, and V. A. Stolupin, Phys. Rev. C **82**, 054619 (2010).
[14] A. J. Koning, S. Hilaire, and S. Goriely, TALYS-1.9 (2017), http://www.TALYS.eu.
[15] H. Jiang, Z. Cui, Y. Hu, J. Liu, Yu. M. Gledenov, E. Sansarbayar, G. Khuukhenkhuu, L. Krupa, and I. Chuprakov, Chin. Phys. C **44**, 114102 (2020).
[16] M. Blatt and V. F. Weisskopf, *Theoretical Nuclear Physics* (John Wiley and Sons, Inc., New York, London, 1952).
[17] G. Khuukhenkhuu *et al.*, Phys. Part. Nucl. Lett. **11**, 749 (2014).
[18] D. G. Gardner and Yu-wen yu, Nucl. Phys. **60**, 49 (1964).
[19] H. A. Bethe, Rev. Mod. Phys. **9**, 69 (1937).
[20] L. Scherk and E. W. Vogt, Can. J. Phys. **46**, 1119 (1968).
[21] Experimental Nuclear Reaction Data EXFOR, http://www-nds.iaea.org/exfor/exfor.html.